BEFIB2012 – Fibre reinforced concrete
Joaquim Barros et al. (Eds)

STEEL FIBRE REINFORCED SELF-COMPACTING CONCRETE FOR LIGHTWEIGHT AND DURABLE PEDESTRIAN BRIDGES: CREEP BEHAVIOUR

Pedro J. D. Mendes[*], Joaquim A. O. Barros[*], Delfina M. F. Gonçalves[†] and José M. Sena-Cruz[*]

[*] ISISE, Dep. Civil Eng., School Eng., University of Minho
Campus de Azurém 4800-058 Guimarães, Portugal
e-mail: pedromendes27@me.com, barros@civil.uminho.pt, jsena@civil.uminho.pt web page: www.isise.net

[†] Civitest company,
4760-042 Vila Nova de Famalicão, Portugal
e-mail: delfinagoncalves@civitest.com, web page: www.civitest.pt

Keywords: Pedestrian bridge; Composites; GFRP pultruded profiles; Fiber Reinforced self-compacting concrete; Creep; Finite element method.

Summary: *In recent years, pedestrian bridges built from composites materials have notably increased. This growth is related to the durability problems of traditional materials, as well as the need for fastest construction times. In this context, fiber reinforced concrete (FRC) becomes an important material in this type of structures, since the ductility, high post-cracking tensile strength, high compressive stiffness and strength of FRC can be combined with the benefits derived from the use of FRP profiles to obtain high performance structural systems. In addition, FRC exhibits a durable behaviour since, in general, does not have corrosion problems.*

In this paper a 12 m length single span pedestrian bridge composed by a Steel Fiber Reinforced Self-Compacting Concrete (SFRSCC) deck and two Glass Fiber Reinforced Polymer (GFRP) pultruded I shape profiles was designed. The SFRSCC deck has a constant thickness of 40 mm and 2000 mm wide and a content of hooked ends steel fibers in its mixture, which ensures the necessary strength and ductility for the acting loads. The high post-cracking tensile strength of the SFRSCC allowed the use of pre-stressed solutions in the bridge structural system, which caused an upward deflection and, consequently, tensile stresses in the SFRSCC deck.

Two prototypes of this structural system were built and monitored in order to assess their long-term deformational behavior when subjected to a loading configuration correspondent to the load combination for the deflection serviceability limit states. The main results are presented and discussed.

1 INTRODUCTION

In the last decades, the materials used in construction of pedestrian bridges were essentially steel, wood and reinforced concrete. The susceptibility of these materials to ageing-damage environmental agents has, in general, a significant impact in the life-cycle costs of a structure, due to its maintenance and rehabilitation. In addition, the need for fastest construction has having a booster effect on the development and use of new structural materials and systems, lighter, with less concerns about maintenance and less exposed to degradation caused by environment agents [1]. These new structural materials, also named by composite materials, were first used in the mid 1950s to reinforce

concrete structures (Rubinsky & Rubinsky, 1954; Wines et al., 1966 cit in [2]). Therefore, an important innovation in bridges construction is the use of self-compacting concrete (SCC), which is a concrete that does not require vibration for placing and compaction. The SCC is highly flowable, without the loss of stability, and is able to flow under its own weight completely filling formwork and achieving full compaction, even in the presence of congested reinforcement [3].

In Europe we can find a significant number of bridges, walls and tunnels built using the SCC technology [4]. In the United States, the SCC application in bridge construction has been very limited [4].

More recently, researchers are developing fiber reinforced self-compacting concrete, FRSCC, which consists in the addition of fibers (typically, steel fibers or synthetic fibers) to the SCC composition. The advantage of this mixture is the possibility of obtaining a new material combining the excellent properties of SCC and fibers [5]. The addition of steel fibers to a cement based composition can increase significantly its post-cracking residual strength, but the fluidity and the workability have a general tendency to decrease. To avoid segregation of FRSCC constituents suitable mix design methodologies should be adopted [6]. According to available research [7-8], corrosion of steel fibers is not a concern, as long as the maximum crack width is limited to 0.25 mm.

Therefore, to appraise the efficiency of combining FRSCC and GFRP materials in the construction of a pedestrian bridge, numerical simulations and an experimental program were carried out. The pedestrian bridge analyzed is composed by two pultruded glass fiber reinforced polymer (GFRP) I shape profiles disposed longitudinally, and connected to a steel fiber reinforced self-compacting concrete (SFRSCC) deck (see Figure 1). The SFRSCC deck is intended to withstand the compressive stresses, and the GFRP profiles will handle the tensile stresses. Steel anchors and an epoxy resin make the connection between both materials. The SFRSCC layer has also the role of increasing the flexural stiffness of this structural concept.

Due to the very small thickness of the concrete layer (40 mm), the deck is quite susceptible to the occurrence of macro-cracks during its curing, handling and assembling processes. Furthermore, if pre-stress or pos-tension strategies are adopted to overcome deflection requirements imposed by code-design recommendations, strains higher than cracking strain can occur in this concrete layer. Therefore, to avoid unacceptable crack patterns and crack widths, a SFRSCC material of relatively high post-cracking residual strength is used for the deck.

(a) (b)

Figure 1 – Pedestrian concept: (a) perspective view and (b) cross-section.

2 MATERIAL PROPERTIES

Table 1 shows the mixture composition of the developed SFRSCC, and Table 2 presents the relevant SFRSCC mechanical and rheological properties. Forty-five kg/m^3 of hooked ends steel fibers of 35 mm length, 0.55 mm diameter and 1100 MPa tensile strength were used. The methodology followed to formulate the SFRSCC composition is mainly based on the following three steps [6]: (i) the proportions of the constituent materials of the binder paste are defined; (ii) the proportions of each aggregate on the final granular skeleton are determined; (iii) binder paste and granular skeleton are mixed in distinct proportions until self-compacting requirements in terms of spread ability, correct flow

velocity, filling ability, blockage and segregation resistance are assured, allowing the determination of the optimum paste content in concrete.

Table 1 – SFRSCC mix proportion per m^3.

Cement [kg]	Limestone filler [kg]	Water [kg]	Superplasticizer [kg]	Fine sand [kg]	River sand [kg]	Crushed stone [kg]	Fibers [kg]
380.54	326.17	126.83	6.09	362.59	574.58	510.05	45.00

Table 2 – Rheological and mechanical properties of the SFRSCC.

Parameter	Value
Slump flow	Diameter =80 cm T50=4 s
V-funnel	T=9 s
L-box	H2/H1=0.8
Compressive strength	59.87 MPa
Tensile strength	10.20 MPa
Young's modulus	32.00 GPa

The GFRP profiles were produced by the pultrusion process and are composed by E-glass fibers embedded in a polyester matrix. In accordance with several tests performed with this type of material [9], the average tensile strength in the direction parallel to the fibers is 500 MPa and the compressive strength in the same direction is 375 MPa. Moreover in the context of this work, two GFRP profiles were tested to evaluate the Young´s modulus, and the value of 34 GPa was obtained.

3 CREEP TESTES

3.1 Pedestrian bridge prototypes

To understand the behavior of the present pedestrian bridge structural system, regarding to the long-term deflection, two prototypes were developed.

The geometry of these prototypes was inspired from the structural system of the pedestrian bridge. However, the prototype length, 6 m, is only half of the original bridge span and the transverse dimension of the SFRSCC deck (0.5 m) is four times smaller than the original bridge. The dimensions of both prototypes involved in the creep tests are equal. Figures 2 and 3 show the dimensions of the prototypes, as well as the support conditions. The motivation to develop two prototypes was to evaluate the influence of two different connection configurations between the SFRSCC deck and the GFRP profiles.

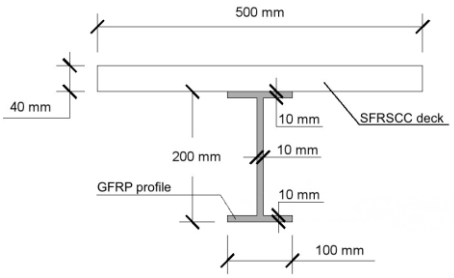

Figure 2 – Cross section of the tested prototypes.

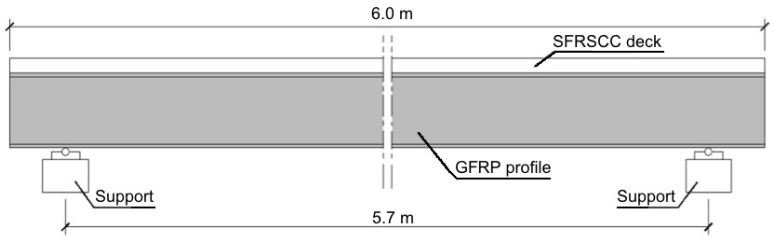

Figure 3 – Side view of the tested prototypes.

The connection between the GFRP profiles and the SFRSCC deck is made by M10 steel anchors, glued to the concrete deck by HIT-HY 150 MAX adhesive, bolted to the GFRP profiles. The surfaces of the concrete deck and the GFRP profiles in contact are also glued by the epoxy adhesive S&P® Resin 220. The anchors are inserted 30 mm into the concrete deck to allow enough contacting area between the anchors and the concrete. The difference between the two prototypes is restricted to the longitudinal distance between the M10 anchors, which is 125 mm in one prototype (PROT_125), and 200 mm in the other (PROT_200). Figure 4 shows the connection configuration, and Figure 5 shows the steps followed to assemble the connection.

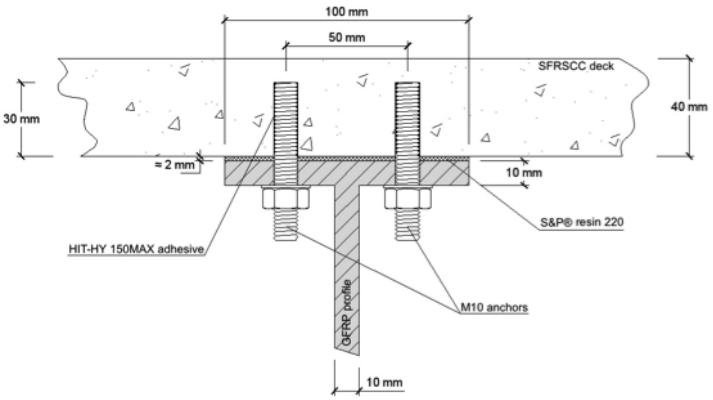

Figure 4 – Configuration of the connection between the SFRSCC deck and the GFRP profiles.

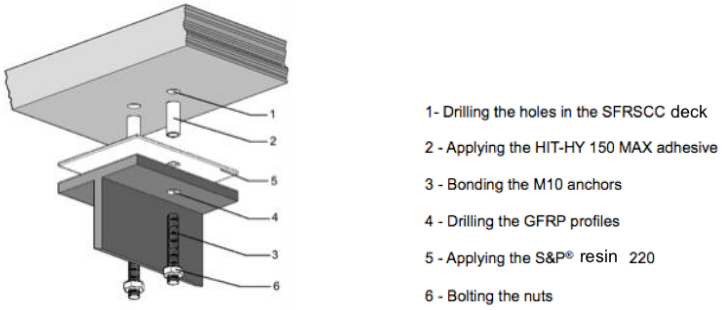

Figure 5 – Steps followed to assemble the connection.

Regarding to the load configuration, the Eurocode 1 part 2 [10] recommends that for the design of pedestrian bridges an uniformly distributed load q_{fk}, calculated according to the equation (1), should be applied only in the unfavorable parts of the influence surface, longitudinally and transversally.

$$q_{fk}=2.0+\frac{120}{L+30} \ [\text{kN/m}^2] \quad ; \quad 2.5 \leq q_{fk} \leq 5.0 \ [\text{kN/m}^2] \tag{1}$$

where *L* is the loaded length in meters. Therefore, from the Eq. (1), and for a loaded length of 5.7 m, results a uniformly distributed load of 5 kN/m^2 applied across the deck surface. To estimate the long-term effects, the Eurocode 0 recommends the quasi-permanent load combination, where 30% of the live load is adopted. However, these recommendations are suitable for reinforced concrete structures and there is no standard for the present type of structures. Hence, the live load used in the creep tests was adjusted to allow a faster evaluation of the creep effect i.e., to appraise the creep in the short time available for this project a live load of 4 kN/m^2 was considered. This uniformly distributed load was materialized by applying cement bags of 40 kg. To measure the mid-span deflection, the strains in the SFRSCC deck and in the GFRP profile, dial gauges were used and positioned at mid-span alignment in four different places in each prototype (see Figure 6). One dial gauge (DI_A, 5 mm stroke and 1 lm accuracy) was fixed on the deck lateral face (at mid height) and was used to measure the concrete strain. The DI_B (5 mm stroke and 1 lm accuracy) was fixed on the top flange of the GFRP profile (centered in the half flange) to measure the strains at this point. To evaluate the strain in the bottom flange of the GFRP profile, the DI_C (10 mm stroke and 10 μm accuracy) was used (positioned at mid-flange). The dial gauge DI_D (40 mm stroke and 10 μm accuracy) measured the mid-span deflection. Note that due to the relative large size of the prototypes, it was not possible to use a climatic chamber to control the exposure temperature and humidity.

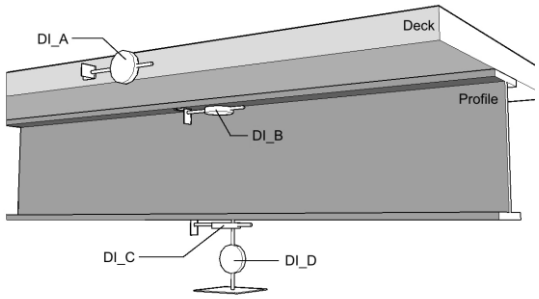

Figure 6 – Position of the dial gauges in the prototype.

3.2 Results

3.2.1 Long-term deflection

The creep tests were carried out between August 10th and September 29th of 2010, with duration of 51 days. When the live load was applied the concrete age was 90 days. During this period the climate was hot (approx.: 32 °C) and dry (approx.: 22%), especially in the first 20 days. On the other hand, in the last 23 days of the live loading period was registered a decrease in the temperature, and an increase in the humidity. The difficulty of assuming perfect symmetric loading conditions may have caused the fell of the PROT_200 from its supports at 21 days of the loading process. Therefore, the PROT_200 values were measured during 21 days, and the PROT_125 values were measured during 51 days.

Figure 7 shows the time-deflection relationship of both prototypes along with the measured temperature.

The evolution of the deflection was similar in both prototypes up to 21st day. At this day the deflection of PROT_125 and PROT_200 was 16.5 mm and 17.1 mm, respectively. The deflection of PROT_125 at 51st day was 18.0 mm. To evaluate the creep influence in the long-term deflection of both prototypes, the short-term deflection was measured (elastic deflection), which was considered as the deflection occurred just after the last cement bag has been applied. The instantaneous deflection of PROT_125 and PROT_200 was 11.9 mm and 11.5 mm, respectively, which is in agreement with the instantaneous elastic deflection predicted by Bernoulli theory of beams (11.6 mm).

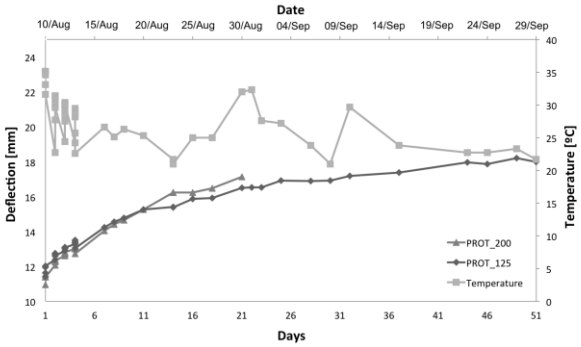

Figure 7 – Time–deflection relationship of PROT_125 and PROT_200.

Figure 8 represents the relationship between the $\mu(t)/\mu(0)$ ratio and time (in days) for both tested prototypes, where $\mu(0)$ and $\mu(t)$ are the instantaneous deflection and the deflection at t days after the live load has been applied, respectively. According to this figure, it is noticeable that similar results were obtained for both prototypes, in terms of creep deflection. The deflection in the PROT_125 has increased 51%, after 51 days, and 48% in the PROT_200 after 21 days, due to creep effect. At 21 days of exposure, the deflection of PROT_125 has increased 38%, hence the difference between both at 21 days of exposure is 10%, which means that, with the anchors spaced by 200 mm, the creep deflection tends to be 10% higher than when spaced by 125 mm.

Figure 9 represents the time variation of the relative flexural stiffness ($EI(t)/(EI(0)$) registered in both prototypes, where $EI(0)$ and $EI(t)$ is the instantaneous elastic flexural stiffness and the flexural stiffness at t days after live load application, respectively.

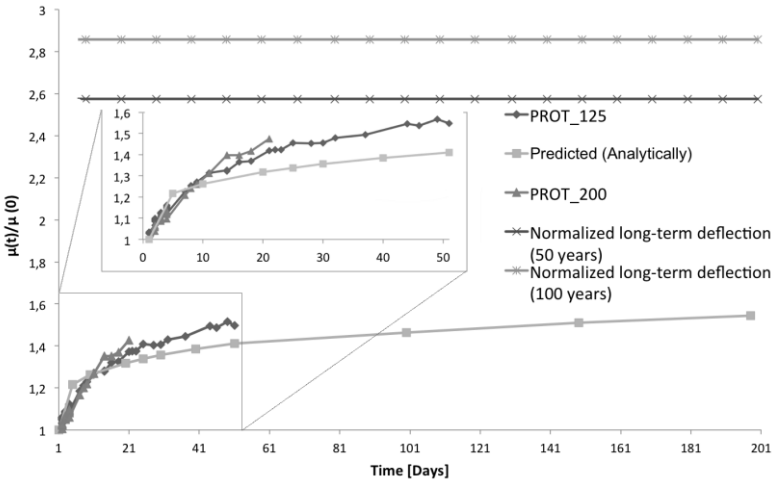

Figure 8 – Creep behavior: experimental and predicted numerical results.

The flexural stiffness was estimated based on the theory of elasticity, according to the load and the deflection obtained.

Due to creep effect, at the end of 21 and 51 days the relative flexural stiffness has decreased 35% and 46%, respectively. In Figure 9 it is also represented the equation:

$$\frac{EI(t)}{EI(0)} = \frac{1+t^{1.11}}{1+1.35 \cdot t^{1.185}} \quad (2)$$

that best fits the experimental data up to 51 days. According to this equation, the *EI(t)/EI(0)* at 50 and 100 years will be 826.1 kN·m^2 and 778.9 kN·m^2, which corresponds to a flexural stiffness that is 35% and 33% of the corresponding instantaneous elastic flexural stiffness.

To estimate the long-term deflection due to creep, the creep behavior of the SFRSCC layer was estimated according to the recommendations of Eurocode 2, part 1 [11] and CEB-FIP Model Code 1990 [12], and the creep behavior of the GFRP was determined adopting the creep law suggested by Bank [13].

Therefore, and regarding to the concrete creep law, to appraise the effective concrete modulus during the time, the Eq. (3) was used, where the creep parameter, $\varphi(t,t_0)$, was calculated using Eq. (4).

$$E_{c,eff} = \frac{E_{cm}}{1+\varphi(t,t_0)} \tag{3}$$

$$\varphi(t,t_0) = \varphi_0 \cdot \beta_c(t - t_0) \tag{4}$$

$$\beta_c(t - t_0) = \left[\frac{(t-t_0)/t_1}{\beta_H+(t-t_0)/t_1}\right]^{0.3} \tag{5}$$

where $E_{e,eff}$ is the effective modulus of elasticity of concrete; E_{cm} is the concrete secant modulus of elasticity at 28 days; φ_0 is the is the notional creep coefficient; $\beta_c(t - t_0)$ is the coefficient to describe the development of creep with time after loading, where t is the time in days, and t_0 is the age of the concrete at time of loading, in days.

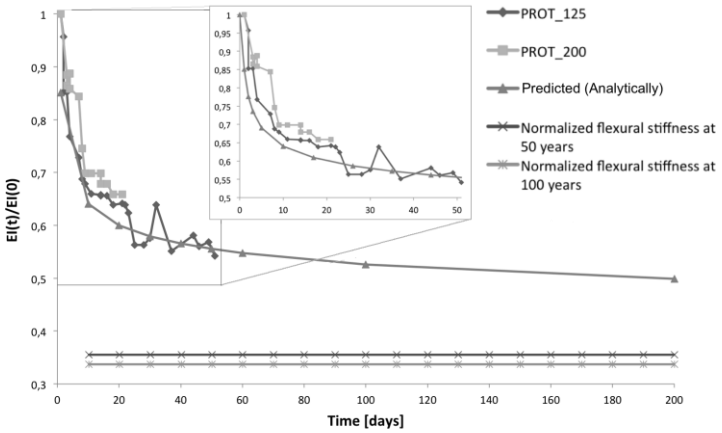

Figure 9 – Evolution of the flexural stiffness: experimental and predicted analytical results.

Regarding to the GFRP profiles, and according to Bank's theory for creep [13], the GFRP longitudinal viscoelastic modulus, E_L^{υ}, should be calculated using the following equation:

$$E_L^{\upsilon} = \frac{E_L}{1+\left(\frac{E_L}{E_L^t}\right)\cdot t^{n_e}} \tag{6}$$

where E_L is the instantaneous modulus (34 GPa); E_L^t is the creep modulus (1241 GPa); t is the time in hours after loading and n_e is the creep rate exponent (0.3).

Using Eqs. (3) to (6), the concrete and the GFRP modulus were calculated for the ages coinciding with records in terms of temperature and humidity, in order to take this information into account in the evaluation of $\beta_c(t - t_0)$, as suggested by CEB-FIP 1990. Knowing $E_{c,eff}$ and E_L^{υ} for the SFRSCC and GFRP profile, respectively, the time-deflection evolution was determined and compared to the values registered experimentally, in Figure 8. It is noticeable that for the first 15 days, the results are very

similar, and for the 51st day the difference between the analytical prediction and the experimental results is only 6% (approximately 1 mm). These results demonstrate that the creep behavior of the bridge prototypes can be reasonably predicted with available analytical models. Therefore, applying this analytical approach to appraise the creep deflection for 50 and 100 years, an increase of 158% and 186% is obtained when compared to the instantaneous deflection, respectively (see Figure 8).

3.2.2 Creep strains and stresses

As previously referred, the dial gauges used to measure the strains were positioned at the concrete deck, GFRP profile top flange and GFRP profile bottom flange (see Figure 6). Figure 10 shows the time-strain relationship for these three analyzed positions and for both tested prototypes. In these figures it is visible that the middle surface of the SFRSCC deck is under compressive strain, while the top and the bottom flange of the GFRP profile are under tensile strains. Table 3 shows the measured values for both prototypes at 21 days and, in the case of the PROT_125, also at 51 days.

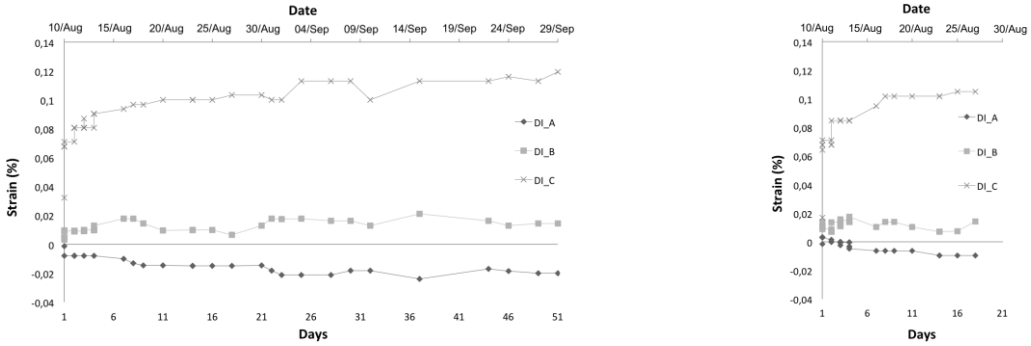

Figure 10 – Time (days) *versus* strain: (a) PROT_125 and (b) PROT_200.

Table 3 – Strains measured and obtained analytically in both prototypes.

Days	PROT_125			PROT_200		
	DI_A	DI_B	DI_C	DI_A	DI_B	DI_C
1	-0.80e-4 (-1.11e-4)	0.9e-4 (0.52e-4)	6.8e-4 (8.01e-4)	-0.6e-4 (-1.11e-4)	0.9e-4 (-0.52e-4)	6.7e-4 (8.01e-4)
21	-1.40e-4 (-1.62e-4)	1.3e-4 (0.93e-4)	10.0e-4 (8.96e-4)	-1.1e-4 (1.62e-4)	1.4e-4 (-0.93e-4)	10.5e-4 (8.96e-4)
51	-2.00e-4 (-1.86e-4)	1.5e-4 (1.13e-4)	11.9e-4 (9.45e-4)	n/a	n/a	n/a
Years	In both Prototypes					
	DI_A		DI_B		DI_C	
50	(-2.82e-4)		(-1.47e-4)		(17.85e-4)	
100	(-2.86e-4)		(-1.35e-4)		(20.08e-4)	

() Values obtained analytically.
Note: negative means compression.

In the first 21 days the results were similar in both prototypes and the differences can be caused by several factors, such as small differences in the loading conditions, the supports/position of the dial gauges, the assemblage of the constituent elements of the prototypes and their materials properties. Therefore, the influence of the longitudinal distance between the M10 anchors on the flexural behavior

at the end of 21 days of loading seems to be not significant. This means that using a small distance between the M10 anchors does not bring any significant benefit in terms of creep deflection for service limit states (SLS). Figures 12 and 13 show the creep influence in the strain diagrams at 21 and 51 days, respectively. The darkest part of the diagram corresponds to the instantaneous strains, while the clearest part corresponds to the long-term strains. The increase percentage of strain that was caused by creep is also indicated in these figures. Note that the compressive strain diagram was represented by a dotted line because there is no certainty if some sliding between SFRSCC deck and the top flange of the GFRP profile has occurred.

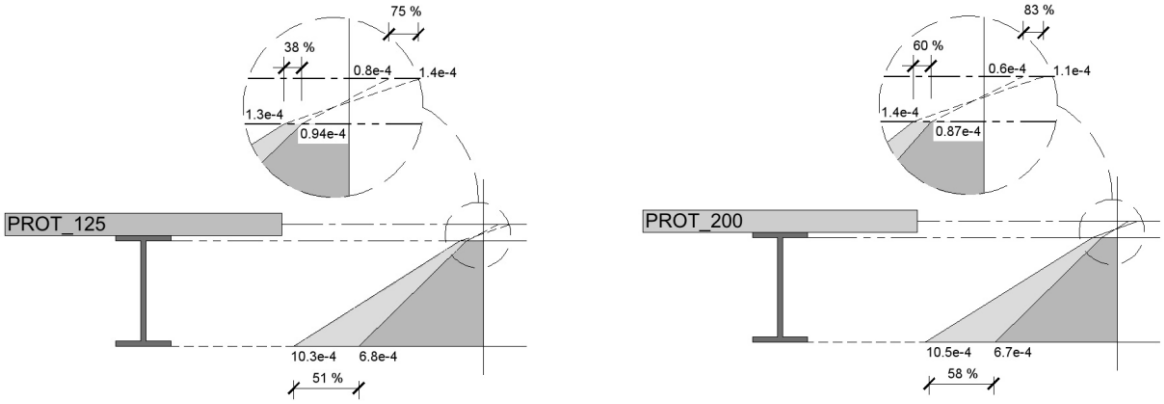

Figure 11 – Influence of creep in the strain profile after 21 days.

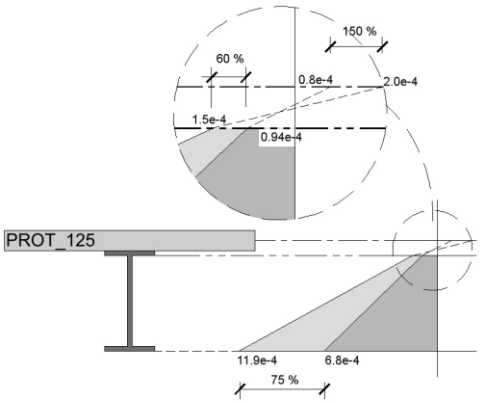

Figure 12 – Influence of creep in the strain profile after 51 days.

In general, similar results were obtained in both prototypes at the end of 21 days of loading (see Figure 10), demonstrating once again that the distance between the M10 anchors has no influence in the flexural behavior for SLS. At the end of 51 days of loading, the strains in PROT_125 have increased more significantly, being the SFRSCC deck the point where the highest increment was measured (150%). The tensile strain in the bottom flange of the GFRP profile has increased 75%, while in the top flange the strain has increased 60%. Using the models based on Eqs (3) to (6), the strains can be estimated at 50 and 100 years. The obtained values are indicated in Table 3. The increase in the compressive strain in the SFRSCC layer at the end of 50 and 100 years is 253% and 258%, respectively. For the tensile strain in the bottom flange, the increase at the end of 50 and 100 years is 163% and 195%, respectively. However, as seen in Table 3, using the previous law's in a FEM based model to predict the long-term strains, the neutral axis position differs from the one obtained in the creep tests. Nonetheless, some slight differences were registered when comparing the values obtained numerically up to the 51th day, which can be justified by the laws' used, i.e., the creep

law used to estimate the effective concrete modulus is suitable for ordinary concretes, and regarding to the creep law for the GFRP profiles, the Bank theory was based in pultruded profiles with 40% of fiber reinforcement, which differ from the ones used in the present paper (62% according to Correia, 2004), hence, this can result in slightly differences. Concluding, these results show that the creep influence, in the long-term strains, is an important factor to the bridge design.

Moreover, from the previous models (Eqs (3) to (6)) and performing FEM analysis, the evolution of the stresses can be estimated at 50 and 100 years. Table 4 shows the instantaneous stresses for both prototypes, and the predicted stresses at the end of 50 and 100 years. These results show that, if instantaneous values are considered for comparison purposes, the stress increment at the end 50 and 100 years is -1.3% and 0.4% for concrete. For the bottom flange of the GFRP profile, and assuming the analytical position of the neutral axis, the increment in the tensile stress is 0.9% and 0.2% for 50 and 100 years.

At 50 and 100 years the stress levels in the SFRSCC deck and GFRP profiles are similar to the corresponding instantaneous ones, and quite inferior to the stress limits recommended for these materials.

Table 4 - Stresses determined and obtained analytically for both prototypes (MPa).

Days	PROT_125			PROT_200		
	DI_A	DI_B	DI_C	DI_A	DI_B	DI_C
1	-2.36	1.66	25.41	-1.26	2.85	21.25
Years	In both prototypes					
	DI_A		DI_B		DI_C	
50	-2.33		-2.14		25.63	
100	-2.35		-1.74		25.45	

Note: Negative means compression

4 FEM BASED ANALYSIS

In the context of the present research project, numerical analysis of the full size pedestrian bridge were carried out, in order to execute parametric studies for the optimization of this structural concept. Three main types of analysis were performed: (i) assuming GFRP profiles connected to a 40 mm thick SFRSCC deck; (ii) using a hybrid profile with CFRP sheets bonded to the bottom flange of the GFRP profile; (iii) using a hybrid profile with pre-stressed CFRP sheets bonded to the bottom flange of the GFRP profile. In all these approaches a 40 mm thick SFRSCC deck was used. Finally, for the connection between GFRP profiles and SFRSCC deck it was investigated the following three different bond conditions: (i) using steel anchors and the epoxy adhesive; (ii) assuming only epoxy adhesive; (iii) assuming only steel anchors. The details of this numerical research can be found elsewhere [14].

5 CONCLUSIONS

In this work a composite solution for a pedestrian bridge of 12 m span is proposed, composed by a deck made by steel fiber reinforced self-compacted concrete (SFRSCC) of 40 mm thickness and 2 m wide, and GFRP ‘‘I’’ shape profiles. To connect the GFRP profiles to the concrete deck, epoxy adhesive and steel anchors (M10) were used. Several studies were performed, experimental and numerical, including creep effect, stress analyses, serviceability and ultimate limit analyses and cross-section optimization.

Creep tests carried out in the two prototypes of the bridge system, showed that using smaller distances between the M10 anchors does not bring any benefit to the bridge behavior, i.e., the long-term deflection of the prototypes was not affected by using a larger distance between the M10

anchors. Nonetheless, the deflection at 51 days of loading was increased 60% due to the creep effect, showing that this is an important phenomenon that should be taken into account in the bridge design. The stresses measured in the creep tests for both materials are far from their ultimate strength. This means that the bridge design is conditioned by service limit state due to the deflection.

The numerical simulations of the bridge revealed that to accomplish the deflection limit imposed by Eurocode 2, the geometry of the GFRP profile should be 550 x 200 x 15 mm^3, maintaining the thickness of the SFRSCC deck constant and equal to 40 mm. Furthermore, the results showed that the stresses in both materials are very similar to the stresses determined experimentally. Based on the numerical research carried out in another work [14], it was verified that using a 450 x 200 x 6.5 mm^3 GFRP profile with a CFRP pre-stressed sheet of 0.50 mm thickness, the deflection limit is also accomplished.

From the numerical and experimental research, it was concluded that the connection between the deck and the profile can be made exclusively by epoxy adhesives, but the long term of these adhesives when subjected to real weathering and to fatigue load conditions should be investigated, along with the dynamic response of the proposed concept.

ACKNOWLEDGEMENTS

This research is part of the research project funded by ADI co-financing FEDER by POFC - COMPETE of QREN Nº 3456 – PONTALUMIS Development of a prototype of a pedestrian bridge in GFRP-ECC concept, involving the Company ALTO – Perfis Pultrudidos, Lda., the ISISE/University of Minho and the ICIST/Technical University of Lisbon. The first author wishes to acknowledge the research grant under this project. The authors also wish to acknowledge the Civitest Company for the conception and development of the steel fiber reinforced self-compacting concrete used in this work, and to Secil, S&P Clever Reinforcement Ibérica, Lda. and Hilti Portugal – Productos e Serviços Lda. for the supplied materials and technical support.

REFERENCES

[1] Correia JP. “GFRP pultruded profiles in civil engineering: hybrid solutions, bonded connections and fire behaviour”. PhD thesis. *Instituto Superior Técnico*, Lisbon; 2008.

[2] ACI Committee 440. “State-of-the-art report on fiber reinforced plastic reinforcement for concrete structures”. *Manual of concrete practice*, American Concrete Institute, Detroit; 1996.

[3] EFCA. EFCA aims. European federation of concrete admixtures associations; 2005. <http://www.efca.info/publications.html> [retrieved 19.02.10].

[4] Ouchi M, Nakamura S-a, Osterberg T, Hallberg S-E, Lwin M. “Applications of self-compacting concrete in Japan, Europe and The United States”. Federal Highway Administration, US Department of Transportation; 2003.

[5] Barros JAO, Pereira EB, Santos SPF. “Lightweight panels of steel fiber reinforced self-compacting concrete”. J Mater Civil Eng 2007;19(4):295–304.

[6] Pereira ENB. “Steel fibre reinforced self-compacting concrete: from material to mechanical behaviour”. Dissertation for pedagogical and scientific aptitude proofs. Department Civil Engineering, University of Minho; 2006. 188 pp. <http://www.civil.uminho.pt/composites>.

[7] Bernard ES. Durability of Fibre-Reinforced Shotcrete. Shotcrete: More Engineering Developments, Taylor and Francis, 2004: 59-64.

[8] Nemegeer D, Vanbrabant J, Stang H. Brite-Euram Program on Steel Fibre Concrete, Durability Corrosion Resistance of Cracked Fibre-Reinforced Concrete. In: Schnütgen B, Vandewalle L, editors. Test and Design Methods for Steel Fibre Reinforced Concrete-Background and Experiences. RILEM Technical Committee 162, TDF Workshop, Proceedings Pro 31, 2003: 47-66.

[9] Correia JP. “Glass fibre reinforced polymer (GFRP) pultruded profiles. Structural behaviour of GFRP-concrete hybrid beams”. Master thesis. *Instituto Superior Técnico*, Lisbon; 2004 [in Portuguese].
[10] CEN/CENELEC. “Eurocode 1: actions on structures – Part 2: Traffic loads on Bridges”. Brussels: CEN; 2003.
[11] CEN/TC250. “Eurocode 2: design of concrete structures – Part 1–1: General rules and rules for buildings”. Brussels: CEN; 2004.
[12] CEB. CEB-FIP model code 1990. Lausanne: Thomas Telford Services; 1993.
[13] Bank LC. “Composites for construction: structural design with FRP materials”. Hoboken: John Wiley & Sons; 2006.
[14] Mendes PJD et al. “Development of a pedestrian bridge with GFRP profiles and fiber reinforced self-compacting concrete deck”. *Compos Struct* (2011).